

# Long Range Temperature Fluctuation in LHD

Shigeru INAGAKI<sup>1,2)</sup>, Tokihiko TOKUZAWA<sup>3)</sup>, Kimitaka ITOH<sup>2,3)</sup>, Katsumi IDA<sup>2,3)</sup>, Sanae-I. ITOH<sup>1,2)</sup>, Naoki TAMURA<sup>3)</sup>, Satoru SAKAKIBARA<sup>3)</sup>, Naohiro KASUYA<sup>3)</sup>, Akihide FUJISAWA<sup>1,2)</sup>, Shin KUBO<sup>3)</sup>, Takashi SHIMOZUMA<sup>3)</sup>, Takeshi IDO<sup>3)</sup>, Seiya NISHIMURA<sup>3)</sup>, Hiroyuki ARAKAWA<sup>4)</sup>, Tatsuya KOBAYASHI<sup>4)</sup>, Masatoshi YAGI<sup>1,2)</sup>, Kenji TANAKA<sup>3)</sup>, Yoshio NAGAYAMA<sup>3)</sup>, Kazuo KAWAHATA<sup>3)</sup>, Shigeru SUDO<sup>3)</sup>, Hiroshi YAMADA<sup>3)</sup>, Akio KOMORI<sup>3)</sup> and LHD Experiment Group

<sup>1)</sup> *Research Institute for Applied Mechanics, Kyushu University, Kasuga 816-8580, Japan*

<sup>2)</sup> *Itoh Research Center for Plasma Turbulence, Kyushu University, Kasuga 816-8580, Japan*

<sup>3)</sup> *National Institute for Fusion Science, Toki 502-5292, Japan*

<sup>4)</sup> *Interdisciplinary Graduate School of Engineering Sciences, Kyushu University, Kasuga 816-8580, Japan*

(Received 31 August 2010 / Accepted 11 January 2011)

We report a detailed correlation technique to identify the long-range temperature fluctuation in the Large Helical Device. Correlation hunting has successfully realized the observation of electron temperature fluctuations, which are characterized by their correlation length comparable to the plasma minor radius, with low frequency of  $\sim 1$ -3 kHz, ballistic radial propagation (at a speed of  $\sim 1$  km/s, of the order of diamagnetic drift velocity), spatial mode number of  $m/n = 1/1$  (or  $2/1$ ), and amplitude of  $\sim 2\%$  at the maximum. Bicoherence analysis confirmed their nonlinear coupling with local microscopic turbulent fluctuations. This long-range temperature fluctuation is a possible carrier of fast propagation in transport processes observed so far. We also comment on the theoretical interpretation.

© 2011 The Japan Society of Plasma Science and Nuclear Fusion Research

Keywords: electron temperature fluctuation, correlation length, transient transport, toroidal plasma, modulational coupling

DOI: 10.1585/pfr.6.1402017

## 1. Introduction

In magnetized toroidal plasmas, it is presumed that local turbulence caused by a local microinstability (e.g. drift instability) drives local transport [1]. In future experiments on thermonuclear fusion, such as the Internal Thermonuclear Experimental Reactor (ITER), the performance and controllability of plasmas are predicted and designed based on the basis of such a presumption. However, the fast radial propagation of temperature perturbations in toroidal plasmas, i.e., the so-called “transient transport problem”, has been observed in many tokamaks and helical devices during the course of the last two decades [2–7]. The temperature perturbation, which is applied to the plasma edge region, propagates inward at a speed that is 10-50 times faster than that expected from diffusive transport models. Fast propagation phenomena have been observed in both L- and H-mode plasmas and plasmas without magnetohydrodynamic (MHD) activities. Thus, the “transient transport problem” is not restricted to a particular state of plasma and is a generic characteristic of plasmas. In plasma physics, this problem is an academic challenge for the comprehensive understanding of turbulence-driven transport. In nuclear fusion research, a fast transport response has a significant impact on the plasma control al-

gorithm in order to maintain stationary burning under the control of heat flux to the divertor. In spite of its importance, this problem has considerably confused the scientists.

Global fluctuation with long distance correlation is a possible candidate to explain the fast propagation phenomena. Avalanche phenomena and nonlinear excitation by the random noise of microturbulence through a statistical process may generate the global fluctuations [8–12]. Mathematically, fractional kinetics has been formulated as a tool to analyze this [13]. Zonal flows are one of the mesoscale fluctuations [14, 15]. Methods for searching mesoscale fluctuations and turbulence anatomy are well developed experimentally [16, 17]. The searching method for macroscale fluctuations, which covers the entire area of plasma, is urgently needed. These theoretical as well as experimental advancements can now be applied to the research of global fluctuations. The measurement of electron cyclotron emissions (ECE) has been developed and used for observations of global dynamics at the onset of a sawtooth crash and of neoclassical tearing modes [18–22]. A few reports have been suggested the existence of low-frequency temperature fluctuations [23–25]; however, the details of these fluctuations, such as their spatiotemporal structure, have not been clarified yet.

author's e-mail: inagaki@riam.kyushu-u.ac.jp

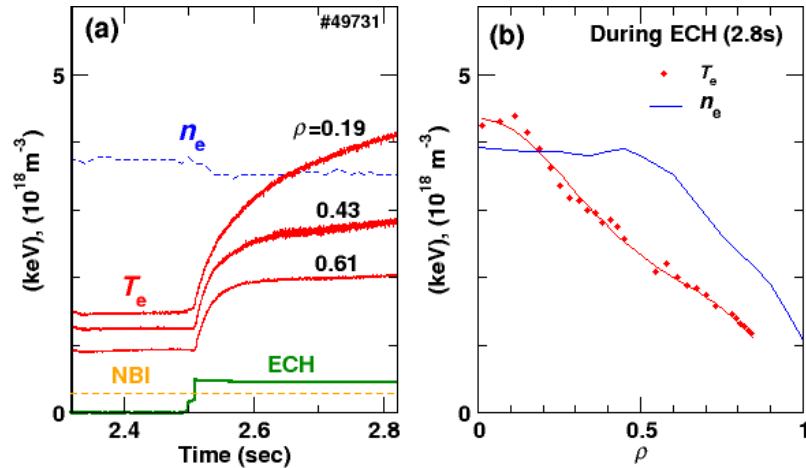


Fig. 1 (a) Typical time evolution of  $T_e$  at three different radii and the line averaged density. (b) Radial profiles of  $T_e$  and  $n_e$  at 2.8 s.

Recently, macroscale low-frequency temperature fluctuations were discovered in the Large Helical Device (LHD) [7] by using global correlation measurements between fluctuations or their envelope obtained from a multichannel ECE system, a microwave reflectometer and a magnetic probe array arranged over the entire range of the torus [26]. We report the details of observations and correlation technique. Global fluctuations have the following features: The radial correlation length of the observed fluctuations is comparable to the plasma minor radius and the mode number is  $m/n = 1/1$  or  $2/1$ , where  $m(n)$  is the poloidal or toroidal mode number. The fluctuation propagates radially with a phase velocity of 1 km/s, which is of the order of the diamagnetic drift velocity. The amplitude of the fluctuation reaches approximately 1% of the averaged temperature at  $\rho = 0.4$ , where  $\rho$  is the normalized average radius. The amplitude has a strong electron temperature,  $T_e$ , dependence,  $T_e^4$ , in the higher temperature region ( $T_e > 2$  keV). Bi-spectrum analysis indicates a non-linear modulational coupling between the global fluctuations and the microscopic fluctuations.

Global fluctuations with long distance correlation have a significant impact on transport phenomena. This discovery verifies that the change in the transport is caused not only by the change in the local plasma parameters but also by the fast propagation of the global fluctuations with long radial correlation. This is the first observation on global fluctuation that plays an important role in the transient transport phenomena.

## 2. Experimental Setup

### 2.1 Target plasma

The experiments were carried out on the LHD, which has a major radius  $R$  of 3.5 m, an averaged minor radius of 0.6 m, and a magnetic field strength  $B_{ax}$  of 2.83 T on the axis. The temporal evolution of the typical discharge presented here is shown in Fig. 1 (a). The target

L-mode plasma was produced with a neutral beam injection of 2 MW, then an electron cyclotron resonant heating (ECRH) of 1 MW was superimposed on the plasma center at  $t = 2.5$  s. During the discharges, the line-averaged density was almost constant at  $\bar{n}_e = 4 \times 10^{18} \text{ m}^{-3}$ , and the central electron temperature,  $T_e(0)$ , was found to increase from 1.5 to 4 keV after the superposition of ECRH. Figure 1 (b) shows the temperature and density profiles at  $t = 2.8$  s, measured with a 28-channel ECE radiometer and a 13-channel far-infrared interferometer [7, 27, 28], respectively.

In the ECRH phase, the volume-averaged  $\beta$  was 0.1% and the electron collision frequency normalized by the bounce frequency of helical ripple-trapped orbit was  $\sim 0.03$ . The plasma had neither MHD activity nor power modulation and was without a transport barrier. The heat diffusivity estimated from the power balance equation at  $t = 2.8$  s is  $\sim 3 \text{ m}^2/\text{s}$  at half of  $\rho$ .

### 2.2 Diagnostics for fluctuations

Global correlation analysis was applied during the quiet period from  $t = 2.7$  to 2.8 s by using an ECE radiometer that provide the radiation temperature ( $T_{\text{rad}}$ ), with supporting fluctuation measurements obtained using an X-mode reflectometer [29] and magnetic field pick-up coils [30]. The locations of these diagnostics are denoted in Fig. 2. The fluctuations in radiation temperature,  $T_{\text{rad}}$ , were measured by the ECE radiometer. A possible difference between  $T_{\text{rad}}$  and  $T_e$  is discussed later. Spatial resolution of the radiometer was 2.5 and 1 cm in the regions of  $\rho < 0.2$  and  $\rho \geq 0.4$ , respectively. Temporal resolution was 10  $\mu\text{s}$ . The detection limit of the fluctuation was  $\sim 1$  eV/kHz in the kHz frequency band because of thermal noise [31]. The frequency of the reflectometer was 78 GHz and the reflecting surface was located at  $\rho \approx 0.4$ -0.43 in this plasma. The temporal resolution was 1  $\mu\text{s}$ . The reflectometer and ECE antennae were located  $72^\circ$  apart in a toroidal direc-

tion, as shown in Fig. 2. The 6-channel magnetic probes were aligned in the toroidal direction and the 4-channel probes were arranged in the poloidal direction. The magnetic fluctuation level for estimation of the mode structure was  $\tilde{b}/B_{ax} \sim 10^{-6}$ .

### 2.3 Measured fluctuations

The  $T_{rad}$  fluctuations,  $\tilde{T}_{rad}$ , were observed with a multichannel ECE radiometer. Figure 3 displays the Fourier spectrum of  $\tilde{T}_{rad}$  before and during the ECH phase at  $\rho = 0.4$ . The spectrum shows an unambiguous peak around a few kHz with  $\sim 1$  kHz bandwidth. At higher frequencies ( $f > 10$  kHz) the spectrum had an  $f^{-1/2}$  dependence, corresponding to random noise [32]. The significant  $T_{rad}$  fluctuations in the narrow band of a few kHz are routinely

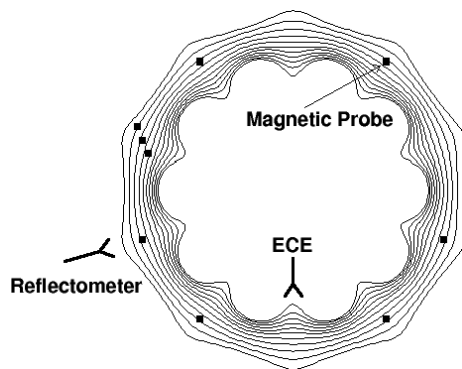


Fig. 2 Contour plot of the magnetic flux surfaces on the equatorial midplane of LHD. Measurement locations of magnetic probes used in this analysis are indicated by filled squares. The reflectometer antenna and the ECE antenna are located  $72^\circ$  apart from each other in a toroidal direction.

observed in the low collisionality region, in which the frequency and amplitude of the fluctuation vary depending on the discharge. The existence of the low-frequency fluctuation was verified.

Density fluctuations with a broad spectrum (1–100 kHz) were observed by the reflectometer. In order to estimate the low-frequency global potential fluctuations that co-exist with the low-frequency global  $T_{rad}$  fluctuations, an envelope of density fluctuations in the high-frequency band was extracted [16]. A high-pass-filter ( $> 100$  kHz) was applied to the reflectometer signal and its envelope was calculated using a Hilbert transform. The high frequency component of the density fluctuation and its envelope are shown in Fig. 4. Here, the envelope signal is defined by  $I_n$ . A large modulation of  $I_n$  was observed

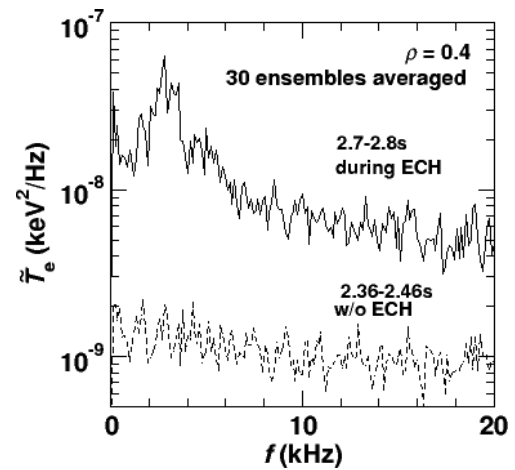


Fig. 3 Fourier spectrum of  $\tilde{T}_{rad}$  at  $\rho = 0.4$  before and during ECH.

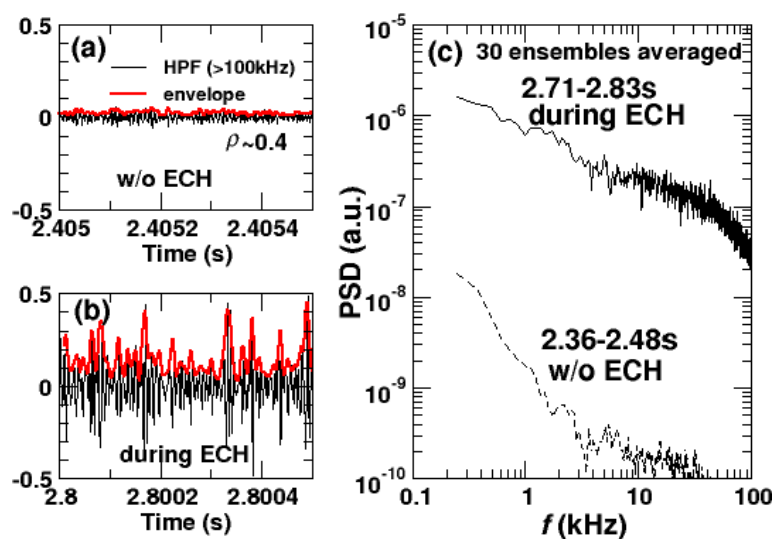


Fig. 4 Typical time evolution of high-pass filtered ( $\geq 100$  kHz) reflectometer signal (black line) and its envelope (red line) (a) before and (b) during the ECH phase. (c) Power spectrum density of the envelope of the reflectometer signal in both cases. The time window for FFT is 8 ms and 30 ensembles are averaged.

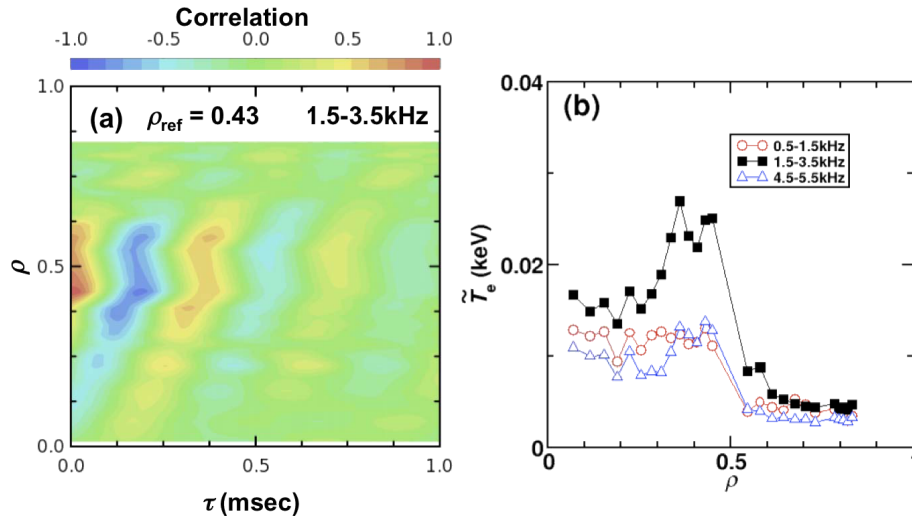


Fig. 5 Contour plot of the cross-correlation function of the low-frequency component (1.5-3.5 kHz) of  $\tilde{T}_{\text{rad}}$  from 28 ECE channels with that of the reference channel at  $\rho = 0.43$ . (b) Radial profile of the amplitude of  $\tilde{T}_{\text{rad}}/T_{\text{rad}}$  in the three characteristic frequency bands.

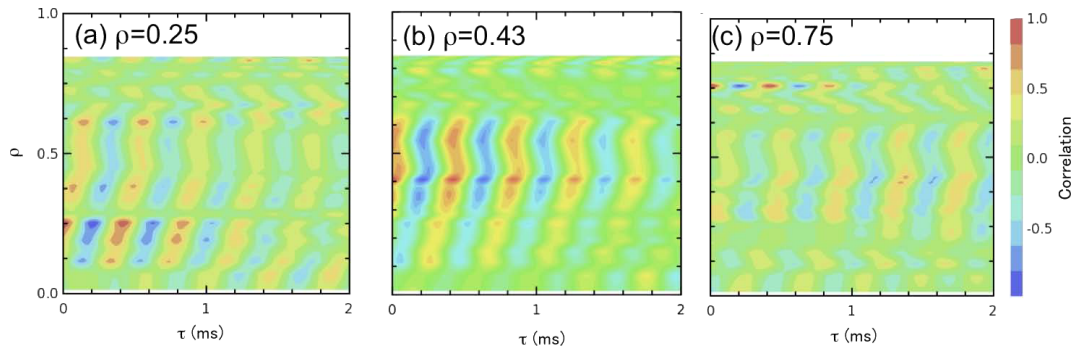


Fig. 6 Contour plots of the cross-correlation function calculated from three different reference channels.

during the ECH phase. The Fourier spectrum of  $I_n$  showed broad peaks around 2 kHz with a full width of the half maximum of  $\sim 1$  kHz during the ECH phase (Fig. 4 (c)). There were no qualitative differences in the spectrum of  $I_n$ , even if the cut-off frequency of the high-pass-filter was changed to 50 kHz.

### 3. Correlation Hunting and Discovery of Long-Range Fluctuation

#### 3.1 Spatiotemporal structure of radiation temperature and long distance correlation

The spatiotemporal structure of the  $T_{\text{rad}}$  fluctuations was determined by a two-point two-time correlation of  $\tilde{T}_{\text{rad}}$  in the range of 1.5-3.5 kHz (a band-pass filter was applied) at different radii. The correlation function between the ECE signals at two different points in space and time is defined as

$$c(\rho, \rho_{\text{ref}}, \tau) = \frac{\langle f(\rho, t)f(\rho_{\text{ref}}, t + \tau) \rangle}{\sqrt{\langle f^2(\rho, t) \rangle \langle f^2(\rho_{\text{ref}}, t) \rangle}},$$

where  $\tau$  is the time lag,  $f(\rho, t)$  is the time series of the ECE channel located at  $\rho$  and  $\langle \rangle$  indicates the temporal averaging defined as  $\langle h(t) \rangle = \frac{1}{T} \int_0^T h(t) dt$ . Figure 5 (a) shows a contour plot of the correlations of  $\tilde{T}_{\text{rad}}$  (which was band-passed in the frequency range of 1.5-3.5 kHz) from 28 ECE channels with that of the reference channel at  $\rho_{\text{ref}} = 0.43$ . The fluctuations have a long radial correlation, which extends from the core to edge region. The radial wavelength was of the order of the plasma radius. The wave propagated from the core to the edge. The propagation was ballistic and not diffusive. The radial phase velocity was extremely fast around  $\rho \sim 0.5$  and  $\sim 1$  km/s on radial average, which is of the order of the diamagnetic drift velocity. The poloidal rotation should be included in the estimation of the radial phase velocity more precisely. The radial profile of the  $\tilde{T}_{\text{rad}}$  amplitude is shown in Fig. 5 (b), and  $\tilde{T}_{\text{rad}}$  exceeds 20 eV at  $\rho \sim 0.4$ . There was no qualitative difference in the correlation functions even if the reference channel was changed from  $\rho = 0.25$  to 0.75, as shown in Fig. 6.

The magnetic probe measured a weak signal in the rel-

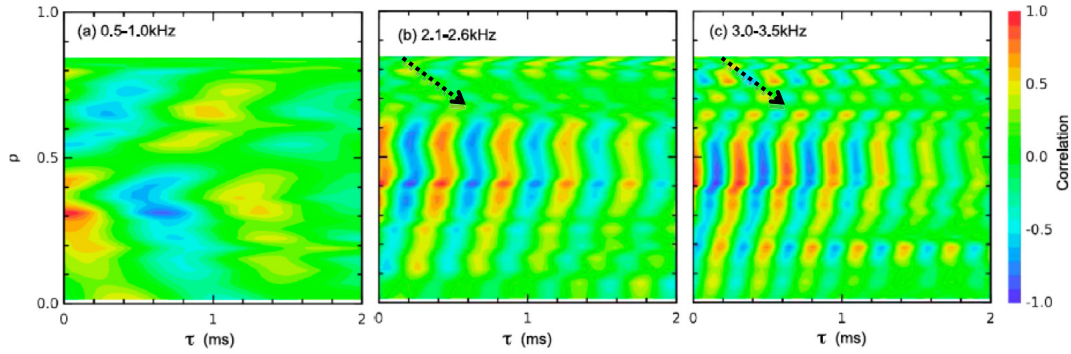


Fig. 8 Contour plots of the cross-correlation function of three different frequency components. Arrows denote propagation of the backward wave.

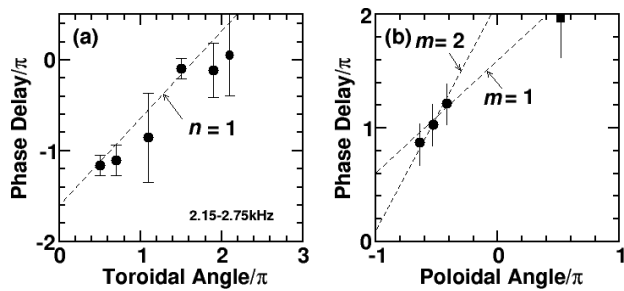


Fig. 7 Cross-phase between  $\tilde{T}_{\text{rad}}$  at  $\rho = 0.4$  and the toroidal magnetic probe array (a) and poloidal array (b).

evant frequency range ( $\tilde{b}/B_{\text{ax}} < 10^{-6}$ ) at the probe position. However, the ECE signals had unambiguous cross-correlation with the magnetic probe signals at  $f = 2.5$  and  $3.5$  kHz. On the basis of this fact, we can conclude that a radially extended global fluctuation accompanies a weak but finite magnetic fluctuation. The toroidal and poloidal mode numbers of  $\tilde{T}_{\text{rad}}$  were estimated by a cross-correlation between the signals from the ECE channel and the magnetic probes. The cross-phase between a 6-channel toroidal array of magnetic probes and an ECE channel (at  $\rho = 0.4$ ) in the frequency range of  $\sim 2.5$  kHz showed that the toroidal mode number is  $n = 1$ , as shown in Fig. 7 (a). If the reference radius of the ECE signal is changed from  $\rho = 0.4$  to other value, the phase difference moves by the amount of the phase difference between the two ECE channels. The conclusion of  $n = 1$  was confirmed by this examination. The cross-phase using the 4-channel poloidal array indicated that the mode propagates in the ion diamagnetic direction and the poloidal mode number is  $m = 1-2$  (Fig. 7 (b)). If the fluctuation structure with  $m/n = 1/1$  or  $2/1$  has a radial wave number,  $k_r$ , comparable with toroidal and poloidal wave numbers, the radial propagation velocity is approximately equal to the diamagnetic drift velocity [33]. A possibility of the long-range fluctuation is discussed later.

### 3.2 Categorization of low-frequency components

Within the present signal-to-noise ratio of the  $T_{\text{rad}}$  measurements, the Fourier spectrum of  $\tilde{T}_{\text{rad}}$  in Fig. 3 suggests the existence of three components of long-range fluctuations. These three components have a strong correlation with  $I_n$  in the wide radial region, as discussed later in Sec. 3.4 (Fig. 10).  $\tilde{T}_{\text{rad}}$  was categorized into three frequency bands ( $f < 1$  kHz,  $f \sim 2$  kHz and  $f \sim 3$  kHz). The two-point two-time correlations of  $\tilde{T}_{\text{rad}}$  were calculated for these three bands and the results are shown in Fig. 8. Here,  $\tilde{T}_{\text{rad}}$  was band-passed in the frequency range of 0.5-1.0 kHz, 2.1-2.6 kHz and 3.0-3.5 kHz and the reference channels were  $\rho_{\text{ref}} = 0.31, 0.43$  and  $0.43$ , respectively. The origin of propagation of the mode with  $f < 1$  kHz was located at  $\rho \sim 0.4$ . As shown in Fig. 6, there was no qualitative difference in propagation features, even if the reference channel was changed. The sub-kHz mode may have qualitatively different features than those of the modes with  $f > 2$  kHz. Details of the sub-kHz mode will be the object of future work; we focus on the fluctuations in the range of 2 kHz or higher. In Figs. 8 (b) and (c), patterns generated by standing waves appear in the region of  $\rho \approx 0.6-0.75$ ; thus a reflection near the plasma boundary ( $\rho \sim 1$ ) was suggested. The phase velocity of backward waves (inwardly propagating waves) was several times lower than the outward velocity. The difference in the propagation pattern at the edge could be due to the interference with the density fluctuation, which is discussed later. This issue will be a topic for our future work.

### 3.3 Dependence of $T_{\text{rad}}$ fluctuation amplitude on $T_e$

In the  $T_e$  rise phase (Fig. 1 (a)), the amplitude of the  $\tilde{T}_{\text{rad}}$  variation depends on the value of  $T_e$ . The timescale of the  $T_e$  rise is  $\sim 100$  ms much longer than that of the representative frequency of  $\tilde{T}_{\text{rad}}$ , and the  $T_e$  rise is considered to be quasi-static. The  $\tilde{T}_{\text{rad}}$  amplitudes at three different radii are illustrated as a function of  $T_e$  in Fig. 9. It displays the amplitudes of  $\tilde{T}_{\text{rad}}$  in the bandwidth of 1.5-3.5 kHz at

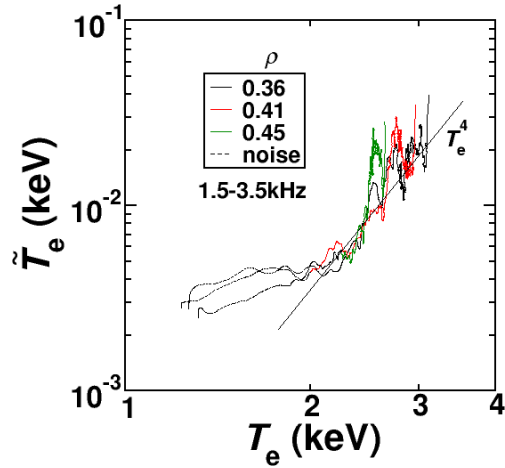


Fig. 9  $T_e$  dependence of the amplitude of  $\tilde{T}_{\text{rad}}$ . The amplitude is averaged over a 10 ms interval.

$\rho = 0.36, 0.41$  and  $0.45$ , where a moving average over 10 ms is applied. The amplitudes in the low temperature region ( $T_e < 2$  keV) were not distinguishable from the noise level. In the high temperature region ( $T_e > 2$  keV), amplitudes of the signal exceeded the noise level and a strong  $T_e$  dependence of  $T_e^4$  appeared. Spontaneous and abrupt jumps (with amplitudes as high as 40 eV) were observed. Details of these jumps need further research and will be discussed in a forthcoming article.

### 3.4 Correlation with modulation of the envelope of density fluctuation and estimation of electrostatic potential fluctuation

The envelope of density fluctuations in the high frequency band indicates the existence of a modulator of microscopic fluctuations, as shown in Fig. 4. A correlation between the modulator and the long-range  $T_{\text{rad}}$  fluctuations was observed. Figure 10 shows a contour plot of the squared cross-coherence between  $\tilde{I}_n$  at  $\rho \approx 0.40-0.43$  and  $\tilde{T}_{\text{rad}}$  of each ECE channel. Significant cross-correlation was demonstrated in the frequency range of 0.2-5 kHz and in the wide radial region during the ECH phase (Fig. 10 (a)). On the other hand, there was no significant correlation when  $T_e$  was low and  $\tilde{T}_{\text{rad}}$  was not distinguishable from noise (Fig. 10 (b)). The existence of fluctuations with a long radial correlation length was verified by the correlation in Fig. 10 (a), which was established by two independent diagnostic methods.

The electrostatic potential,  $\Delta\phi$  of the long-range fluctuation was estimated from the envelope  $I_n$ . The study of disparate-scale interactions provided the estimate  $\tilde{I}_n(f)/\langle I_n \rangle \sim f_{\text{micro}} f^{-1} k_r L_n (e\Delta\phi/T_e)$ , where  $\langle I_n \rangle$  is the mean of the envelope of microscopic fluctuations,  $f_{\text{micro}}$  is the frequency of microscopic fluctuations,  $L_n$  is the scale length of the density gradient and  $f$  and  $k_r$  are the frequency and radial wave numbers, respectively, of the long-

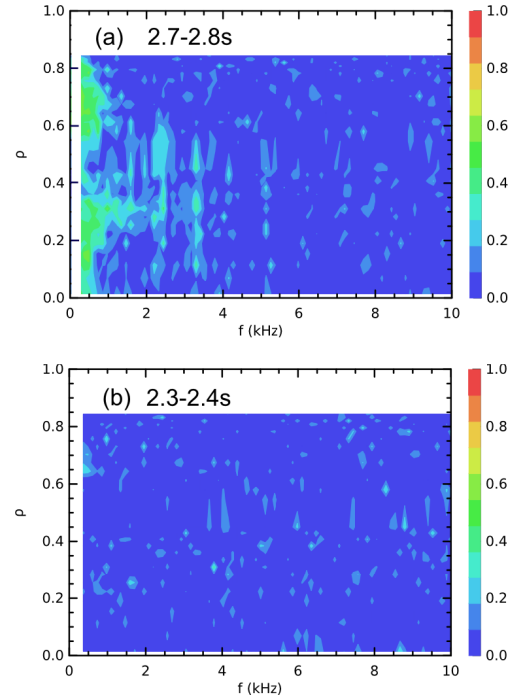


Fig. 10 Contour plot of the squared coherence between the envelope of the reflectometer signal and the 28-channel ECE signals in the space of frequency versus radial location of each ECE channel (a) during and (b) before ECH phase. Measurement location of reflectometer is  $\rho \approx 0.40-0.43$ .

range perturbation [14] (experimental validation is given in Ref. [16]). The time evolution of the envelope of microscopic density fluctuations was observed in the frequency range of 1.5-3.5 kHz. The ratio  $\tilde{I}_n/\langle I_n \rangle \sim 0.3$  was obtained. By substituting the observed values  $\tilde{I}_n/\langle I_n \rangle \sim 0.3$  and  $k_r L_n \sim 1$  for  $f_{\text{micro}} \sim 100$  kHz, an estimate of  $e\Delta\phi/T_e \sim 0.01$  in the relevant frequency range of  $\sim 2.5$  kHz can be obtained. This fact suggests that the electrostatic potential fluctuation comparable to  $\tilde{T}_{\text{rad}}$  exists ( $e\Delta\phi \sim \tilde{T}_{\text{rad}}$ ). The heavy ion beam probe (HIBP) in LHD (injected beam ion energy is 6 MV) cannot resolve the potential fluctuation of the order of 1-10 V till date [34]. This point must be examined in the future experiment.

### 3.5 Nonlinear coupling with microscopic fluctuations

No modulation was observed in the heating power around 2.5 kHz. The observed long-range fluctuations are not considered to be caused by external heating. To verify the nonlinear excitation of the long-range fluctuation by strong microinstability, bicoherence analysis was applied [35]. Careful consideration of statistical convergence is required in the bicoherence analysis. The statistical convergence was confirmed in this study.

Bicoherence of each ECE signal showed nonlinear coupling of the long-range  $\tilde{T}_{\text{rad}}$  fluctuations (1.5-3.5 kHz) with their second harmonics. However, there was no sig-

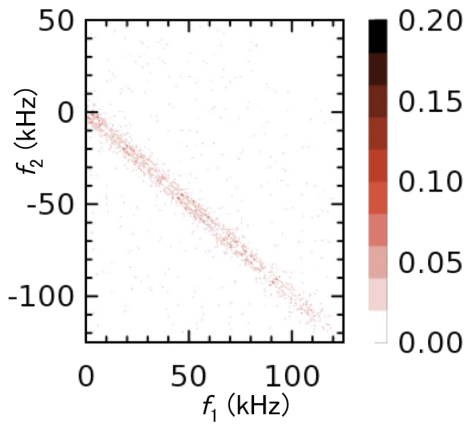


Fig. 11 Contour plot of squared cross-bicoherence between  $n_e$  and  $T_e$  fluctuations for 2.6-2.8 s. The time window for FFT is 8 ms and 360 ensembles are averaged. The three-channel ECE signals ( $\rho = 0.4, 0.43, 0.45$ ) are averaged to increase the number of ensembles.

nificant bicoherence between the 1.5-3.5 kHz components and the high-frequency components of  $\tilde{T}_{\text{rad}}$  due to extensive noise in the high-frequency region ( $\geq 10$  kHz). Nonlinear interactions between these long-range and microscopic fluctuations were identified by cross-bispectral analysis. Cross-bispectrum  $Z$  for three waves (1,2 and 3) is defined as  $Z = \langle \hat{n}_1 \hat{n}_2 \hat{T}_3^* \rangle$ , where  $\langle \rangle$  denotes ensemble averaging and the frequency satisfies the matching condition  $f_1 + f_2 = f_3$ , and  $\hat{n}$  and  $\hat{T}$  are the Fourier transforms of the density and  $T_{\text{rad}}$  fluctuations, respectively. The cross-bicoherence  $z$  is defined as

$$z^2 = \frac{Z^2}{\langle |\hat{n}_1 \hat{n}_2|^2 \rangle \langle |\hat{T}_3|^2 \rangle}.$$

The cross-bicoherence is used to quantify the extent of the phase coupling between  $\tilde{n}_e$  and  $\tilde{T}_{\text{rad}}$ . In Fig. 11, the significant cross-bicoherence is observed along a line in the form  $f_1 + f_2 \sim \pm 2.5$  kHz. This means that  $\tilde{T}_{\text{rad}}$  around 2.5 kHz couples nonlinearly with  $\tilde{n}_e(f_1)$  and  $\tilde{n}_e(f_2)$  where  $f_1 + f_2 \sim \pm 2.5$  kHz is satisfied. This result is consistent with the fact that the high-frequency components of  $\tilde{n}_e$  are modulated in the frequency range of 1-3 kHz as shown in Fig. 4(c). The biphase under the condition of  $f_1 + f_2 = f_3 = 2.5$  kHz is scattered; however, it is distributed around a single value; thus the existence of modulational coupling of microscopic fluctuations is suggested.

Because the observed long-range  $\tilde{T}_{\text{rad}}$  fluctuation is considered to be linearly stable, the existence of nonlinear coupling with microscopic fluctuations suggests an energy transfer from microscopic fluctuations to the large-scale fluctuation. The direction of the energy transfer between microscopic fluctuations and the large-scale fluctuation has not been identified yet. However, observation of the Reynolds stress makes it possible to study the energy transfer process [36], which is the objective of future work.

## 4. Contribution to Transport

### 4.1 Random walk model and contribution to transport in stationary state

The impact of this large-scale fluctuation on transport in a stationary state was evaluated. Noting the fact that the radial excursion of the equicontour  $T_{\text{rad}} \sim 5$  mm was significantly lesser than the radial wavelength, we saw that the Kubo number was significantly smaller than one. Therefore, the contribution to transport in the stationary state may be evaluated using a random walk model. The step size of  $\sim 5$  mm estimated from the radial excursion and the decorrelation rate of  $10^4 \text{ s}^{-1}$  estimated from the half width at the half maximum of the spectrum peak  $\sim 1$  kHz yield an effective diffusion coefficient of  $D_{\text{eff}} \sim 0.2 \text{ m}^2/\text{s}$ . This is a small portion (of the order of  $10^{-1}$ ) of the heat diffusivity estimated from a power balance equation in a stationary state.

### 4.2 Transient transport

However, for the transient transport, this fluctuation plays a dominant role in the fast response, because the change of the amplitude of this mode (i.e., the change of  $D_{\text{eff}}$ ) has a ballistic propagation of the order of 0.1 ms as shown in Fig. 5(a). This value is 50-100 times faster than that expected from diffusive transport models. The change of the large-scale fluctuation will induce the change of  $D_{\text{eff}}$ , which propagates across the plasma column within 0.1 ms [10]. This timescale could explain the abrupt change of the transport observed as non-local phenomena in the LHD [7, 37]. In Refs. [7, 37], a fast timescale for propagation of the order of 1 ms has been reported. The speed of propagation of the order of the diamagnetic drift velocity is sufficiently fast to explain the abrupt change of transport observed in many toroidal plasmas [2-7]. The large-scale  $\tilde{T}_{\text{rad}}$  fluctuation is one of the entities capable of producing a rapid transient response. The relation to the improvement of confinement has been studied and discussed in Ref. [26].

## 5. Discussion

### 5.1 Radiation temperature

The  $T_{\text{rad}}$  and  $T_e$  are related as  $T_{\text{rad}} = (1 - \exp(-\tau))T_e$ , where  $\tau$  is the optical thickness and  $\tau \propto n_e T_e$ . Hence, the  $T_{\text{rad}}$  fluctuations are affected by the  $T_e$  fluctuations,  $\tilde{T}_e$ , and the density fluctuations,  $\tilde{n}_e$ , as  $\tilde{T}_{\text{rad}}/T_{\text{rad}} = (1 + C)/\tilde{T}_e T_e + C\tilde{n}_e/n_e$ , where  $C = \tau/(\exp(\tau) - 1)$ . In the present experiment, the density fluctuation level was difficult to estimate; thus discussion is required for the precise estimation of the  $T_e$  fluctuation level. We can discuss the approximate level of the  $T_e$  fluctuation by considering the optical thickness. In this experiment,  $\tau > 4$  is satisfied in the plasma core [38]. If there is no  $T_e$  fluctuation, then the observed value of  $\tilde{T}_{\text{rad}}/T_{\text{rad}} \sim 0.01$  indicates that  $\tilde{n}_e/n_e$  exceeds 0.1. There is no evidence of such large density fluctuations and they are difficult to generate in the flat density profile re-

gion. A working hypothesis that the dominant contribution to  $\tilde{T}_{\text{rad}}$  comes from  $\tilde{T}_e$  is allowed. The optical thickness is sufficiently large ( $\sim 3$ ) at  $\rho \sim 0.5$ . In the edge region ( $\rho \sim 0.8$ ),  $\tau \sim 1$  holds in order for  $\tilde{T}_{\text{rad}}$  to be influenced by the density fluctuations. Thus, there is a possibility that the difference of radial propagation between the core and edge regions (Fig. 5 (a)) stems from the optical thickness.

For the fluctuations propagating with the diamagnetic drift velocity, the temperature variation is significantly smaller than the density variation, i.e.,  $(\tilde{T}_e/T_e)/(\tilde{n}_e/n_e) \sim O(\omega/k_{\parallel}v_{\text{th}})$ , where  $v_{\text{th}}$  is the electron thermal velocity and  $k_{\parallel}$  is the parallel wave number, in slab plasmas because of temperature relaxation through transit electrons. However, the variation can be  $O(1)$  in toroidal plasmas when the electrons are trapped [1]. In this experiment, the plasma was in the collisionless regime; thus the fluctuations were considered to be accompanied by the temperature variations because of the response of the trapped electrons. The influence of the orbit width on the observed correlation length was negligible; therefore it was not essential. The orbit width of a helically trapped electron was  $\sim 3$  cm and the trapped electrons moved radially  $\sim \Delta/a < 0.05$  during a period of large-scale fluctuations ( $\sim 1/2.5$  kHz), which was significantly less than the radial correlation length of  $\tilde{T}_{\text{rad}}$  fluctuations (see Fig. 5 (a)). On the basis of this fact, we can conclude that the long distance radial correlation was real and was not caused by the motion of trapped electrons.

## 5.2 Comparison with MHD mode

The magnetic fluctuation level, which accompanies the  $\tilde{T}_{\text{rad}}$  fluctuation, was compared with the fluctuation level that was observed during the MHD activity with a similar mode structure. Large magnetic fluctuations ( $\tilde{b}/B_{\text{ax}} \approx 10^{-5}$ - $10^{-4}$  outside plasma boundary) have been observed when interchange modes ( $m/n = 2/1$ ) are excited in high- $\beta$  ( $\beta > 2\%$ - $3\%$ ) LHD plasmas [30]. For such large-amplitude magnetic perturbations, the deformation of the magnetic flux surface is estimated to be  $\sim 3$  cm in the core plasma [39]. Magnetic fluctuation, which was observed here, was 30 or more times less. The temperature variation, which was estimated using the observed magnetic fluctuation amplitude and assuming a frozen-in condition, was less than 2.6 eV. This estimated value was significantly smaller than the observed variation (30 eV). The large-scale  $\tilde{T}_{\text{rad}}$  fluctuations were not caused by MHD instability such as interchange modes. In addition, the radial propagation patterns (Figs. 5 (a) and 8) are not explained by the interchange modes.

## 5.3 Comparison with theory

A theoretical study on low-frequency temperature fluctuations has not been accomplished; yet it is compared to the recent studies of microscale and mesoscale fluctuations [14]. However, the possibility of non-linear excita-

tion has been suggested and its importance is widely recognized.

Pumping of linearly stable modes and quasimodes in the low- $n$  drift wave frequency range by unstable microscopic fluctuations is a possible excitation mechanism of fluctuation with an  $n = 1$  mode structure [10]. One of the candidates for this low-frequency fluctuation is a linearly stable dissipative trapped-ion mode (DTIM) [40]. The relation  $\omega_{\text{hb},i} > |k_{\parallel}v_{\text{th},i}| > \omega_{\text{b},i} > \omega \geq \nu_{\text{heff},i} > \nu_{\text{eff},i}$  was satisfied for the fluctuation of interest, where  $v_{\text{th},i}$  and  $v_i$  are ion thermal speed and collision frequency, respectively,  $\omega_{\text{hb},i}$  and  $\omega_{\text{b},i}$  are the bounce frequencies of helically and toroidally trapped ions, respectively, and  $\nu_{\text{heff},i}$  and  $\nu_{\text{eff},i}$  are the effective collision frequencies of helically and toroidally trapped ions, respectively. Because of the relation  $|k_{\parallel}v_{\text{th},i}| > \omega$ , the response of transit ions is given by the Boltzmann distribution. The collision frequency was greater than the gradient- $B$  drift frequency ( $\nu_{\text{heff},i} > \nu_{\text{eff},i} > \omega_{\text{DM}}$ ). These relations indicate that the observed frequency is in the DTIM region. The dispersion relation was given as

$$\omega_{\text{DTIM}} \approx \sqrt{\varepsilon}/2\omega^*, \text{ and } \gamma = \varepsilon\nu_{\text{eff},e}^{-1}\omega^{*2}/4 - \varepsilon^{-1}\nu_{\text{eff},i},$$

where  $\omega^*$  is the drift frequency of the wave and  $\varepsilon = r/R$  [40].

Our observations were compared to this theoretical prediction. In this experiment,  $\gamma$  was estimated as  $\gamma \sim -10^3 \text{ s}^{-1}$  and the DTIM was predicted to be stable. The frequency of the observed mode was 1.5-3.5 kHz in the laboratory frame. To estimate the frequency in the plasma frame, the Doppler shift because of  $\mathbf{E} \times \mathbf{B}$  drift should be considered. In low-density ECH plasmas, the positive electrostatic potential of the order of  $T_e$  is observed [34]. Considering the positive mean electrostatic potential (of the order of  $T_e$ ), a Doppler shift of  $\omega_{\mathbf{E} \times \mathbf{B}} \sim -m \times 10^4 \text{ s}^{-1}$  occurs in the laboratory frame. Thus, the dispersion relation in the laboratory frame is predicted to be

$$\omega_{\text{lab}} = \omega_{\text{DTIM}} + \omega_{\mathbf{E} \times \mathbf{B}} \sim -(1 + \sqrt{\varepsilon}/2)m \times 10^4 \text{ s}^{-1}.$$

The observed frequency was close to  $\omega_{\text{lab}}$  and the spectral width of excited fluctuations ( $\sim 1$  kHz) was close to the damping rate  $\gamma$  [10]. The observed mode was close to that predicted as the linearly stable DTIM. We suppose here that the linearly stable DTIM is excited by nonlinear coupling with microscopic fluctuations.

The avalanche phenomena of heat transport with  $n = 0$  mode structure has also been predicted [11, 12]. In this case, the propagation speed of the avalanche is also of the order of the diamagnetic drift velocity. The  $n = 0$  component in the  $\tilde{T}_{\text{rad}}$  fluctuations has not been observed. The correlation between an avalanche and the very low-frequency (10-100 Hz) temperature fluctuations has been discussed in DIII-D [25]. The relationship between the  $\tilde{T}_{\text{rad}}$  fluctuations in a sub-kHz band (Fig. 8 (a)) and the fluctuations in a 1.5-3.5 kHz band (Fig. 3 (b)) are the subjects of future experiments.

## 6. Conclusion

In conclusion, we have discovered the large-scale and low-frequency electron temperature fluctuations in LHD plasmas. We obtain the following experimental results: (i) the radial correlation length of the fluctuations is comparable to the plasma radius and the mode number is  $m/n = 1/1$  or  $2/1$ , (ii) the fluctuations propagate radially at a ballistic speed of 1 km/s, which is of the order of the diamagnetic drift velocity, (iii) the amplitude of fluctuation has a strong  $T_e$  dependence and (iv) the fluctuations are nonlinearly coupled with the microscopic fluctuations. One of candidates for the large-scale fluctuations is the linearly stable DTIM. The fluctuations have substantial impact on turbulent transport and could be a leading player in transient transport response phenomena.

The existence of low-frequency temperature fluctuations has been suggested in many toroidal plasmas [23–25]. Fluctuations with a long distance correlation can be observed using the correlation technique reported in this study.

For reliable control of plasmas in thermonuclear fusion reactors, the establishment of algorithms, which consider not only the diffusive propagation but also the ballistic propagation of change of the transport, is required. The discovery that is reported in this article serves as a basis for these important challenges.

## Acknowledgment

We thank Prof. P. H. Diamond, Dr. T. Yamada and Dr. Y. Nagashima for the useful discussions. We are grateful to the technical group in NIFS for their excellent support. This work is partly supported by a Grant-in-Aid for Scientific Research of JSPF, Japan (21224014, 19360148) and by the collaboration programs of NIFS (NIFS07KOAP017, NIFS10KOAP023) and of the RIAM of Kyushu University and Asada Science Foundation.

- [1] J.A. Wesson, *Tokamaks* (Oxford, 1987).
- [2] L. Laurent, *Plasma Phys. Control. Fusion* **28**, 85 (1986).
- [3] E.D. Fredrickson *et al.*, *Phys. Rev. Lett.* **65**, 2869 (1990).
- [4] J.G. Cordey *et al.*, *Plasma Phys. Control. Fusion* **36**, A267 (1994).
- [5] K.W. Gentle *et al.*, *Phys. Plasmas* **2**, 2292 (1995).
- [6] U. Stroth *et al.*, *Plasma Phys. Control. Fusion* **38**, 1087 (1996).
- [7] S. Inagaki *et al.*, *Nucl. Fusion* **46**, 133 (2006).
- [8] T. Iwasaki *et al.*, *J. Phys. Soc. Japan* **68**, 478 (1999).
- [9] K. Itoh and S.-I. Itoh, *Plasma Phys. Control. Fusion* **44**, A367 (2002).
- [10] S.-I. Itoh and K. Itoh, *Plasma Phys. Control. Fusion* **43**, 1055 (2001).
- [11] P.H. Diamond and T.S. Hahm, *Phys. Plasmas* **2**, 3640 (1995).
- [12] X. Garbet and R. Waltz, *Phys. Plasmas* **5**, 2836 (1998).
- [13] G. Zaslavsky, *Hamiltonian Chaos and Fractional Dynamics* (Oxford University Press, Oxford, 2005).
- [14] P.H. Diamond, S.-I. Itoh, K. Itoh, T.S. Hahm, *Plasma Phys. Control. Fusion* **47**, R35 (2005).
- [15] A. Fujisawa *et al.*, *Phys. Rev. Lett.* **93**, 165002 (2004).
- [16] Y. Nagashima *et al.*, *Plasma Phys. Control. Fusion* **49**, 1611 (2007).
- [17] T. Yamada *et al.*, *Nature Phys.* **4**, 721 (2008).
- [18] A.E. Costley, *Plasma Phys. Control. Fusion* **30**, 1455 (1988).
- [19] H.K. Park *et al.*, *Phys. Rev. Lett.* **96**, 195003 (2006).
- [20] A. Isayama *et al.*, *Nucl. Fusion* **47**, 773 (2007).
- [21] Y. Nagayama *et al.*, *Phys. Rev. Lett.* **90**, 205001 (2003).
- [22] H. Zohm *et al.*, *Phys. Plasmas* **8**, 2009 (2001).
- [23] S. Sattler and H.J. Hartfuss, *Phys. Rev. Lett.* **72**, 653 (1994).
- [24] C. Watts and C.F. Gandy, *Phys. Rev. Lett.* **75**, 1759 (1995).
- [25] P.A. Politzer, *Phys. Rev. Lett.* **84**, 1192 (2000).
- [26] S. Inagaki *et al.*, 23th IAEA Fusion Energy Conference (Daejeon), IAEA, Vienna (2010) EXC/7-4Ra.
- [27] K. Kawahata *et al.*, *Rev. Sci. Instrum.* **74**, 1449 (2003).
- [28] K. Tanaka *et al.*, *Nucl. Fusion* **46**, 110 (2006).
- [29] T. Tokuzawa *et al.*, Proc. 31st EPS conf., P5-114, London, UK (2004).
- [30] S. Sakakibara *et al.*, *Nucl. Fusion* **41**, 1177 (2001).
- [31] H.J. Hartfuss, T. Geist and M. Hirsch, *Plasma Phys. Control. Fusion* **39**, 1693 (1997).
- [32] A. Cavallo *et al.*, *Plasma Phys. Contr. Fusion* **23**, 61 (1981).
- [33] Kasuya *et al.*, *J. Plasma Fusion Res. SERIES* **9**, 523 (2010).
- [34] T. Ido *et al.*, *Plasma Sci. Technol.* **11**, 460 (2009).
- [35] Y.C. Kim and E.J. Powers, *IEEE Trans. Plasma Sci.*, PS-7:120 (1979).
- [36] Y. Nagashima, S.-I. Itoh, S. Shinohara, M. Fukao, A. Fujisawa *et al.*, *Phys. Plasmas* **16**, 020706 (2009).
- [37] N. Tamura *et al.*, *Nucl. Fusion* **47**, 449 (2007).
- [38] S. Kubo *et al.*, AIP conference proceedings: ICPP2002 **669**, 187 (2003).
- [39] A. Isayama *et al.*, *Plasma Phys. Control. Fusion* **48**, L45 (2006).
- [40] B.B. Kadomtsev and O.P. Pogutse, *Nucl. Fusion* **11**, 67 (1971).